Robotica: (2021) volume 39, pp. 217–232. © The Author(s), 2020. Published by Cambridge University Press.
doi:10.1017/S0263574720000338

A Multi-Priority Controller for Industrial Macro-Micro Manipulation

Emre Uzunoğlu†*, Enver Tatlıcıoğlu‡ and Mehmet İ. Can Dede†

†*Department of Mechanical Engineering, Izmir Institute of Technology, Izmir, Turkey*
E-mail: candede@iyte.edu.tr
‡*Department of Electrical and Electronics Engineering, Izmir Institute of Technology, Izmir, Turkey*
E-mail: envertatlicioglu@iyte.edu.tr

(Accepted April 22, 2020. First published online: May 19, 2020)

SUMMARY
In this study, a control algorithm is proposed and evaluated for a special type of kinematically redundant manipulator. This manipulator is comprised of two mechanisms, macro and micro mechanisms, with distinct acceleration and work space characteristics. A control algorithm is devised to minimize the task completion duration and the overall actuator effort with respect to the conventional manipulator. A general framework multi-priority controller for macro-micro manipulators is introduced by utilizing virtual dynamics, which is introduced in null-space projection to achieve secondary tasks. The proposed controller is evaluated on a simulation model based on a previously constructed macro-micro manipulator for planar laser cutting. Task completion duration and the total actuator effort are investigated and the results are compared.

KEYWORDS: Redundant manipulators; Robot dynamics; Control of robotic systems; Macro-micro manipulation; Multi-priority control; Computed torque control.

1. Introduction

Kinematically redundant manipulators can provide the task designer with an infinite number of solutions that can achieve the same primary task, since they possess more degrees of freedom (DoF) than required to execute a given task. Self-motion of the redundant manipulator, which has no effect on the primary task,[1] has been used to achieve a variety of subtasks, for example, singularity avoidance and minimizing total joint motion. Several redundancy resolution algorithms have been proposed in the literature that allow the ability to optimize for various criteria using subtasks without interfering with the primary/top task. Redundancy resolution in velocity level by making use of the pseudo-inverse approach has been widely used in various subtask controls such as singularity avoidance,[2] joint velocity minimization,[3] obstacle avoidance,[4] mechanical joint limit avoidance[5] and manipulability.[6] These controllers have based their redundancy resolution algorithms on only kinematic parameters. Additionally, multi-priority controllers which base their redundancy resolution algorithms on dynamic parameters with torque controllers were developed.[7,8] In terms of dynamic consistency, a wide overview of torque controllers which utilize redundancy projections is given and analyzed in ref. [9].

A special set of kinematic redundancy is formed by the use of different mechanisms that inherently have distinct capabilities. Such systems can be distinctly categorized under macro-micro manipulation (MMM) because of their unique configurations. MMM, as its name suggests, is comprised of

* Corresponding author. E-mail: emreuzunoglu@iyte.edu.tr

a macro mechanism with a relatively larger work space and a lightweight micro mechanism dealing with confined motions with relatively higher dynamic capabilities. Concisely, mounting a micro manipulator to the end of a macro manipulator can provide fine adjustment of errors in position or force and thereby enhance accuracy and/or inertial characteristics of the overall manipulator while maintaining a large work space. In this regard, the human upper limb can be observed and imitated as a macro-micro system, especially for tasks such as writing,[10] where the shoulder and elbow joints act as a macro manipulator for coarse positioning, and wrist and fingers deal with finer motions.

The development of the MMM originated from the need for better accuracy and dynamic performance. To the best knowledge of the authors, the MMM was first mentioned explicitly in the study of Sharon and Hardt[11] in 1984. Khatib, in his work,[12] analyzed the control and effective inertial characteristics of MMM. In ref. [13], a general control framework for macro/mini manipulator to improve the force and compliant motion control performance is introduced. In ref. [14], hybrid position/force controllers are used on a mechanism which is the combination of a flexible macro and a rigid micro mechanism. Henceforth, the MMM became a field of study for improving positional and force accuracy as well as dexterous manipulation.

In terms of applications, many studies are conducted to enhance the performance of systems by means of accuracy and force control. An MMM welding robot based on the vision navigation is designed in ref. [15], which is used for seam tracking. The control is achieved by the task space division method in which motion is planned for the macro manipulator, while the micro manipulator is used to compensate the tracking errors in real time. In ref. [16], a general control framework for the macro/mini manipulator to improve the force and compliant motion control is introduced. The experimental system in this study comprises 7-DoF Mitsubishi PA-IO as the macro manipulator and 1-DoF voice coil as the mini manipulator. A force/position controller is devised so that it could reduce the impact when the manipulator makes contact with the workpiece. In this case, the micro manipulator is used to regulate the contact forces during the motion of the macro manipulator. MMM control architecture is developed in ref. [17] to enhance the accuracy of robotic machining. An industrial robot, KUKA model KR125, is used as the macro manipulator, while an external piezo-actuated compensation mechanism is used as the micro manipulator. This integrated system is reported to offer significantly higher bandwidth control of the relative position between the tool and the workpiece. The experimental results show that the proposed approach offers higher accuracy, with up to eight times improvement in the milling operation.

Another approach that utilizes MMM is shown to enhance the acceleration capability of the total system by adding a lightweight micro manipulator to a conventional machine. Trumpf company devised a solution in their planar laser cutting machine called Trumatic 7000 to increase the acceleration of the machine by adding additional axes alongside the X- and Y-axes, namely, making the configuration of the machine $XY + xy$.[18] Prima Power Company, from Italy, designed Syncrono Series planar laser cutting machines with two additional axes. Syncrono has the capability of reaching a combined acceleration of 6 g. In this system, the conventional machine axes (X, Y) which can be named as the macro manipulator axes are used to position laser head for macro displacements, and the additional two axes (u and v), which can be named as the micro manipulator axes, are used to move the laser head in a relatively smaller work space.[19,20]

The MMM that is used in this study is a simplified model of the kinematically redundant machine in ref. [21], which is designed for the planar laser cutting operation. Similar to the applications mentioned above, the MMM concept is implemented by adding a micro mechanism at the distal end of a conventional Cartesian manipulator (an x-y table). However, the parallel mechanism used for the micro manipulation and redundancy resolution algorithms used in this study is different from the previous examples in the industry. The agility of the relatively smaller sized parallel mechanism with lower inertia with respect to the macro mechanism is used to enhance the total acceleration capability of the system while the work space dimensions are preserved. In this previous study, a trajectory generation scheme with an off-line task division method and an online compensation to generate the micro mechanism's motion trajectory is proposed and employed on an industrial laser cutting machine.[21,22] The main novelty of the study presented in this article is that it limits the maximum acceleration of the macro manipulator within the desired acceleration bounds during the operation without the need for an iterative procedure as presented in ref. [22]. The proposed methodology also results in the minimization of the total actuation effort.

https://doi.org/10.1017/S0263574720000338 Published online by Cambridge University Press

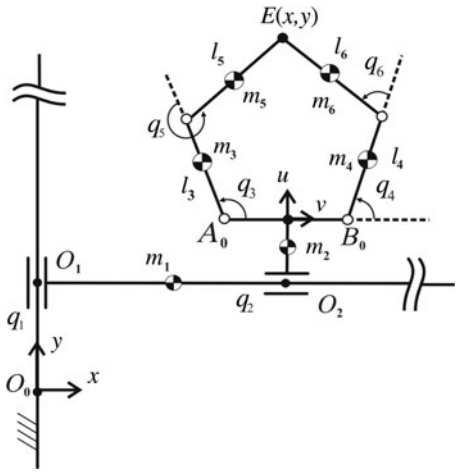

Fig. 1. Model of the macro-micro manipulator (MMM).

The proposed method is a multi-priority control where the first priority is end-effector's motion trajectory tracking and the secondary priority is limiting the maximum acceleration of the macro manipulator to the desired limits while not violating the work space boundaries of the micro manipulator. Redundancy is resolved by designing the null-space controller utilizing a simplified dynamic model of the proposed MMM.

In the first section, the derivation of the dynamic model of the MMM is given. Also, kinematic and dynamic properties of the model are listed. In the following section, the controller designed for the MMM is explained. The redundancy resolution algorithm to regulate the acceleration and work space of the macro and micro manipulators is proposed along with the optimization of the parameters of this algorithm. A simulation test is prepared that has MMM model parameters similar to ref. [21] and the same trajectory as the previous experimental study.[22] The proposed redundancy resolution algorithm is tested in simulations, and the obtained test results are discussed in the conclusions section.

2. Model of the Macro-Micro Manipulator

In this section, a simplified model of the MMM concept that was used for the planar laser cutting machine[21,22] is introduced. To make use of inertial properties of macro-micro mechanisms, assessed specifications on the design of the MMM is given as follows:

1. The macro manipulator has larger work space with 1 g acceleration limit.
2. Micro manipulator is lightweight and has a smaller work space with better acceleration capabilities.

The MMM devised in the study comprises a Cartesian prismatic planar macro manipulator and a five-bar parallel micro manipulator. The Cartesian manipulator has a work space of 1000 × 1500 mm and a planar mechanism devised to use 100 × 150 mm free from kinematic singularities. The mechanism's kinematic structure is represented in Fig. 1. q_1 and q_2 are Cartesian macro mechanism's prismatic joints and q_3 and q_4 are micro mechanisms active revolute joints of five bars. Due to the closed chain, parallel mechanism's q_5 and q_6 joints are passive. Consequently, given a desired trajectory on planar space, the manipulator has two extra DoF. Therefore, in addition to the main objective, which is to follow end-effector trajectory, a secondary objective can be planned by using extra DoF. The dynamic model developed is defined in a compact and structured form and is used to implement a computed torque control method with the novel secondary-task definition for redundancy resolution. However, the computation of the dynamics of the parallel micro mechanism is more complicated than serial macro mechanisms because of their closed-form structure. The model of the mechanism with constraints is derived utilizing reduced-order model method as proposed in refs. [23, 24].

For the model given in Fig. 1, kinematic and dynamic parameters of the MMM in ref. [21] are listed in Table I. Links 1 and 2 are the macro manipulator's links in Cartesian configuration, which is a conventional *x*-*y* table in planar laser cutting machines. In the micro manipulator, five-bar parallel

https://doi.org/10.1017/S0263574720000338 Published online by Cambridge University Press

Table I. Kinematic and dynamic parameters of MMM used in simulations.

	Link length/maximum travel distance (mm)	**Center of Mass (mm)**	**Mass (kg)**	**Moment of inertia about the z-axis (kgmm^2)**
Link 1	1500 (max)	750.2	422.49	1,020,718.61
Link 2	1000 (max)	100	29.87	36,363.92
Link 3/Link 4	150	80.35	3.40	1800.02
Link 5/Link 6	150	82.66	3.91	1312.99

mechanism's Links 3 and 6 are identical to Links 4 and 5, respectively, which shows that they have the same kinematic and dynamic parameters. The length A_0B_0 given in Fig. 1 is chosen to be zero in simulations to be consistent with the actual MMM in ref. [21]. Global axes are represented by x_e and y_e, where end-effector's motions are defined, while the micro manipulator's axes are indicated with u and v on its base frame. The coordinate of five-bar mechanism's workspace middle position is chosen at [0 0.212] m with respect to its base frame.

The model of the closed chain mechanical system can be designed by subjecting constraints to the open-loop model. The 2-DoF five-bar linkage closed-loop mechanism is constructed from two open-chain serial links, and the holonomic system is governed by the following differential equation:

$$\boldsymbol{\tau}' = \boldsymbol{M}'(\boldsymbol{q}')\ddot{\boldsymbol{q}}' + \boldsymbol{N}'(\boldsymbol{q}', \dot{\boldsymbol{q}}')\dot{\boldsymbol{q}}' + \boldsymbol{G}'(\boldsymbol{q}') \tag{1}$$

$$\boldsymbol{q}' = [\, q_1 \; q_2 \; q_3 \; q_4 \; q_5 \; q_6 \,]^T, \quad \dot{\boldsymbol{q}}' = [\, \dot{q}_1 \; \dot{q}_2 \; \dot{q}_3 \; \dot{q}_4 \; \dot{q}_5 \; \dot{q}_6 \,]^T \tag{2}$$

where $\boldsymbol{q}'$ is the vector of generalized coordinates of the manipulator including the passive joints on the five bars and τ' is the corresponding computed torques. $\boldsymbol{M}'(\boldsymbol{q}') \in \mathbb{R}^{6x6}$ is the generalized inertia matrix, $\boldsymbol{N}'(\boldsymbol{q}', \dot{\boldsymbol{q}}') \in \mathbb{R}^{6x6}$ is a matrix including centrifugal and Coriolis terms, and $\boldsymbol{G}'(\boldsymbol{q}') \in \mathbb{R}^6$ is gravity term that are acquired using the Lagrangian method. After obtaining equations of open-chain dynamics, a reduced model in the form of Eq. (3) can be extracted by subjecting it to constraints as follows:

$$\boldsymbol{\tau} = \boldsymbol{M}(\boldsymbol{q}')\ddot{\boldsymbol{q}} + \boldsymbol{N}(\boldsymbol{q}', \dot{\boldsymbol{q}}')\dot{\boldsymbol{q}} + \boldsymbol{G}(\boldsymbol{q}') \tag{3}$$

$$\dot{\boldsymbol{q}}' = \boldsymbol{\rho}(\boldsymbol{q}')\dot{\boldsymbol{q}}, \boldsymbol{q}' = \boldsymbol{\sigma}(\boldsymbol{q}) \tag{4}$$

$$\boldsymbol{q} = \begin{bmatrix} q_1 \\ q_2 \\ q_3 \\ q_4 \end{bmatrix}, \dot{\boldsymbol{q}} = \begin{bmatrix} \dot{q}_1 \\ \dot{q}_2 \\ \dot{q}_3 \\ \dot{q}_4 \end{bmatrix}, \ddot{\boldsymbol{q}} = \begin{bmatrix} \ddot{q}_1 \\ \ddot{q}_2 \\ \ddot{q}_3 \\ \ddot{q}_4 \end{bmatrix} \tag{5}$$

$$\boldsymbol{M}(\boldsymbol{q}') = \boldsymbol{\rho}(\boldsymbol{q}')^T \boldsymbol{M}'(\boldsymbol{q}')\boldsymbol{\rho}(\boldsymbol{q}') \tag{6}$$

$$\boldsymbol{N}(\boldsymbol{q}', \dot{\boldsymbol{q}}') = \boldsymbol{\rho}(\boldsymbol{q}')^T \boldsymbol{N}'(\boldsymbol{q}', \dot{\boldsymbol{q}}')\boldsymbol{\rho}(\boldsymbol{q}') + \boldsymbol{\rho}(\boldsymbol{q}')^T \boldsymbol{M}'(\boldsymbol{q}')\dot{\boldsymbol{\rho}}(\boldsymbol{q}', \dot{\boldsymbol{q}}') \tag{7}$$

$$\boldsymbol{G}(\boldsymbol{q}') = \boldsymbol{\rho}(\boldsymbol{q}')^T \boldsymbol{G}'(\boldsymbol{q}') \tag{8}$$

Using the constraint equation, the parameterization with $\boldsymbol{q}' = \boldsymbol{\sigma}(\boldsymbol{q})$ is implicit and requires solving a differential equation. For a five-bar parallel mechanism, equations can be computed analytically. The determination of $\boldsymbol{M}(\boldsymbol{q}') \in \mathbb{R}^{4x4}, \boldsymbol{N}(\boldsymbol{q}', \dot{\boldsymbol{q}}') \in \mathbb{R}^{4x4}, \boldsymbol{G}(\boldsymbol{q}') \in \mathbb{R}^4, \boldsymbol{\rho}(\boldsymbol{q}') \in \mathbb{R}^{4x6}, \dot{\boldsymbol{\rho}}(\boldsymbol{q}', \dot{\boldsymbol{q}}')) \in \mathbb{R}^{4x6}$, and $\boldsymbol{\sigma}(\boldsymbol{q}) \in \mathbb{R}^6$ for the five bars are calculated as given in ref. [24]. The constrained equations are given in the equation below. Therefore, $\boldsymbol{\sigma}(\boldsymbol{q}) = [\, \boldsymbol{\varphi} \boldsymbol{q}]$ is obtained by constrained equations and active joint positions. $\boldsymbol{\rho}(\boldsymbol{q}')$ and $\dot{\boldsymbol{\rho}}(\boldsymbol{q}', \dot{\boldsymbol{q}}')$ are calculated by taking the time derivative of $\boldsymbol{\sigma}(\boldsymbol{q})$.

$$\boldsymbol{\varphi} = \begin{bmatrix} l_3\cos(q_3) + l_5\cos(q_3 + q_5) - l_4\cos(q_4) - l_6\cos(q_4 + q_6) \\ l_3\sin(q_3) + l_5\sin(q_3 + q_5) - l_4\sin(q_4) - l_6\sin(q_4 + q_6) \end{bmatrix} \tag{9}$$

https://doi.org/10.1017/S0263574720000338 Published online by Cambridge University Press

Redundant manipulator has a Jacobian matrix $\boldsymbol{J} \in \mathbb{R}^{2x4}$.

$$\boldsymbol{J} = \begin{bmatrix} 0 & 1 & -\dfrac{l_3 \sin(q_4+q_6)\sin(q_5)}{\sin(q_3+q_5-q_4-q_6)} & \dfrac{l_3 \sin(q_3+q_5)\sin(q_6)}{\sin(q_3+q_5-q_4-q_6)} \\ 1 & 0 & \dfrac{l_4 \cos(q_4+q_6)\sin(q_5)}{\sin(q_3+q_5-q_4-q_6)} & \dfrac{-l_4 \cos(q_3+q_5)\sin(q_6)}{\sin(q_3+q_5-q_4-q_6)} \end{bmatrix} \tag{10}$$

The task space motion of MMM is represented in Cartesian space with $\boldsymbol{x}$. The relationships of manipulator end-effector velocity and acceleration are described as:

$$\begin{aligned} \dot{\boldsymbol{x}} &= \boldsymbol{J}\dot{\boldsymbol{q}} \\ \ddot{\boldsymbol{x}} &= \boldsymbol{J}\ddot{\boldsymbol{q}} + \dot{\boldsymbol{J}}\dot{\boldsymbol{q}} \\ \dot{\boldsymbol{q}} &= \boldsymbol{J}^{+}\dot{\boldsymbol{x}} + \dot{\boldsymbol{q}}_N \\ \ddot{\boldsymbol{q}} &= \boldsymbol{J}^{+}(\ddot{\boldsymbol{x}} - \dot{\boldsymbol{J}}\dot{\boldsymbol{q}}) + \ddot{\boldsymbol{q}}_N \end{aligned} \tag{11}$$

where $\dot{\boldsymbol{q}} \in \mathbb{R}^4$, $\ddot{\boldsymbol{q}} \in \mathbb{R}^4$ joint velocity and acceleration vectors, $\dot{\boldsymbol{q}}_N \in \mathbb{R}^4$, $\ddot{\boldsymbol{q}}_N \in \mathbb{R}^{4x6}$ are joint space projections to the null space and $\dot{\boldsymbol{x}} \in \mathbb{R}^2$, $\ddot{\boldsymbol{x}} \in \mathbb{R}^2$ are task space velocity and acceleration. The pseudo-inverse of Jacobian matrix denoted by $\boldsymbol{J}^{+} \in \mathbb{R}^{4x2}$ is defined when $\boldsymbol{J}$ has full rank.

3. The Control Law

The computed torque method is used to control the MMM. The control input torque, $\boldsymbol{\tau}$, is formulated in Eq. (12) as in ref. [25], in which the term $\boldsymbol{J}^{+}(\ddot{\boldsymbol{x}}_d + \boldsymbol{K}_v\dot{\boldsymbol{e}} + \boldsymbol{K}_p\boldsymbol{e} - \dot{\boldsymbol{J}}\dot{\boldsymbol{q}})$ ensures the primary objective which is trajectory tracking. The vector $\boldsymbol{\phi}_N \in \mathbb{R}^4$ is in the null space of the Jacobian matrix which is $(\boldsymbol{I} - \boldsymbol{J}^{+}\boldsymbol{J})$ and obtained by multiplying a secondary objective function with the null-space projection matrix. It is proven in ref. [25] that the main task, which can be also named as the primary task, is not affected by any arbitrary demands associated with the null-space vector. Also, gravitational terms are neglected since the planar mechanism does not make any motion against gravity.

$$\boldsymbol{\tau} = \boldsymbol{M}(\boldsymbol{q}')\{\boldsymbol{J}^{+}(\ddot{\boldsymbol{x}}_d + \boldsymbol{K}_v\dot{\boldsymbol{e}} + \boldsymbol{K}_p\boldsymbol{e} - \dot{\boldsymbol{J}}\dot{\boldsymbol{q}}) + \boldsymbol{\phi}_N\} + \boldsymbol{N}(\boldsymbol{q}', \dot{\boldsymbol{q}}') \tag{12}$$

where $\boldsymbol{K}_v \in \mathbb{R}^{2x2}$ and $\boldsymbol{K}_p \in \mathbb{R}^{2x2}$ are constant diagonal gain matrices. Error vectors $\boldsymbol{e}$ and $\dot{\boldsymbol{e}}$ are computed with the desired task trajectory $\boldsymbol{x}_d, \dot{\boldsymbol{x}}_d \in \mathbb{R}^2$ and end-effector $\boldsymbol{x}, \dot{\boldsymbol{x}} \in \mathbb{R}^2$ motions.

$$\boldsymbol{e} = \boldsymbol{x}_d - \boldsymbol{x}, \dot{\boldsymbol{e}} = \dot{\boldsymbol{x}}_d - \dot{\boldsymbol{x}} \tag{13}$$

It should be noticed that that in addition to primary objective controller commands which includes (task-space) command accelerations $\ddot{\boldsymbol{x}}_d$ and the null-space command $\boldsymbol{\phi}_N$, the components of Coriolis and centrifugal forces, $\boldsymbol{N}(\boldsymbol{q}', \dot{\boldsymbol{q}}')$, are completely compensated in the control Eq. (12) to ensure stability. The stability proof of the overall control algorithm is based on the task-priority-based controllers using pseudo-inverse, which was used in ref. [25] to prove the stability of the overall system for any vector of $\boldsymbol{\phi}_N$ which is projected in the null space.

The closed-loop system is given by Eq. (14) is reduced to Eq. (15).

$$\boldsymbol{M}(\boldsymbol{q}')\ddot{\boldsymbol{q}} + \boldsymbol{N}(\boldsymbol{q}', \dot{\boldsymbol{q}}') = \boldsymbol{M}(\boldsymbol{q}')\{\boldsymbol{J}^{+}(\ddot{\boldsymbol{x}}_d + \boldsymbol{K}_v\dot{\boldsymbol{e}} + \boldsymbol{K}_p\boldsymbol{e} - \dot{\boldsymbol{J}}\dot{\boldsymbol{q}}) + \boldsymbol{\phi}_N\} + \boldsymbol{N}(\boldsymbol{q}', \dot{\boldsymbol{q}}') \tag{14}$$

$$\ddot{\boldsymbol{q}} = \boldsymbol{J}^{+}(\ddot{\boldsymbol{x}}_d + \boldsymbol{K}_v\dot{\boldsymbol{e}} + \boldsymbol{K}_p\boldsymbol{e} - \dot{\boldsymbol{J}}\dot{\boldsymbol{q}}) + \boldsymbol{\phi}_N \tag{15}$$

Equating (11) and (15) results in the following expression

$$\boldsymbol{J}^{+}(\ddot{\boldsymbol{e}} + \boldsymbol{K}_v\dot{\boldsymbol{e}} + \boldsymbol{K}_p\boldsymbol{e}) = \ddot{\boldsymbol{q}}_N - \boldsymbol{\phi}_N \tag{16}$$

where $\ddot{\boldsymbol{q}}_N - \boldsymbol{\phi}_N$ belongs to the null space of $\boldsymbol{J}$ and $\boldsymbol{J}$ has full rank. Later Eq. (16) is multiplied with $\boldsymbol{J}$.

$$(\ddot{\boldsymbol{e}} + \boldsymbol{K}_v\dot{\boldsymbol{e}} + \boldsymbol{K}_p\boldsymbol{e}) = \boldsymbol{0} \tag{17}$$

Linear analysis tools can be used to show that error, $\boldsymbol{e}$, goes to zero exponentially with the use of constant positive definite diagonal gain matrices. It should also be noted that the micro mechanism is singularity free as long as the work space boundary, which is set as 100×150 mm, is not violated.

https://doi.org/10.1017/S0263574720000338 Published online by Cambridge University Press

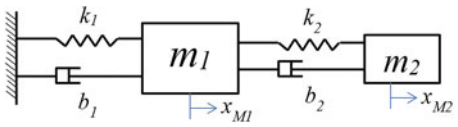

Fig. 2. Double mass-spring-damper model representation for secondary dynamics.

The torque demands for secondary task are decoupled by using null space of the Jacobian. To achieve a stable system behavior in the null space of the system, the impedance-like controller's stability should be issued. The defined virtual inertia $\boldsymbol{M_d}$, damping $\boldsymbol{B_d}$, and stiffness $\boldsymbol{K_d}$ determine the behavior of the robot when subjected to secondary control inputs. The controller used in null space:

$$\ddot{\boldsymbol{x}}_{\boldsymbol{M}} = \ddot{\boldsymbol{x}}_{\boldsymbol{Md}} + \boldsymbol{M}_{\boldsymbol{d}}^{-\mathbf{1}}[(\boldsymbol{B}_{\boldsymbol{d}}\dot{\tilde{\boldsymbol{x}}} + \boldsymbol{K}_{\boldsymbol{d}}\tilde{\boldsymbol{x}}) - \boldsymbol{F}_{\boldsymbol{e}}]$$

To analyze the stability properties of the equation above, Lyapunov candidate function is created:

$$V(\dot{\tilde{\boldsymbol{x}}}, \tilde{\boldsymbol{x}}, t) = \frac{1}{2}\dot{\tilde{\boldsymbol{x}}}^{\boldsymbol{T}}\boldsymbol{M}_{\boldsymbol{d}}\dot{\tilde{\boldsymbol{x}}} + \frac{1}{2}\tilde{\boldsymbol{x}}^{\boldsymbol{T}}\boldsymbol{K}_{\boldsymbol{d}}\tilde{\boldsymbol{x}}$$

Differentiating $V(\dot{\tilde{\boldsymbol{x}}}, \tilde{\boldsymbol{x}}, t)$ with constant $\boldsymbol{M_d}$ and $\boldsymbol{K_d}$ yields:

$$\begin{aligned}\dot{V}(\dot{\tilde{\boldsymbol{x}}}, \tilde{\boldsymbol{x}}, t) &= \dot{\tilde{\boldsymbol{x}}}^{\boldsymbol{T}}\boldsymbol{M}_{\boldsymbol{d}}\ddot{\tilde{\boldsymbol{x}}} + \tilde{\boldsymbol{x}}^{\boldsymbol{T}}\boldsymbol{K}_{\boldsymbol{d}}\dot{\tilde{\boldsymbol{x}}} \\ &= \dot{\tilde{\boldsymbol{x}}}^{\boldsymbol{T}}(-\boldsymbol{B}_{\boldsymbol{d}}\dot{\tilde{\boldsymbol{x}}} - \boldsymbol{K}_{\boldsymbol{d}}\tilde{\boldsymbol{x}}) + \tilde{\boldsymbol{x}}^{\boldsymbol{T}}\boldsymbol{K}_{\boldsymbol{d}}\dot{\tilde{\boldsymbol{x}}} \\ &= -\dot{\tilde{\boldsymbol{x}}}^{\boldsymbol{T}}\boldsymbol{B}_{\boldsymbol{d}}\dot{\tilde{\boldsymbol{x}}}\end{aligned}$$

It can be concluded that the stability is preserved as $\boldsymbol{B_d}$ is assigned as a positive definite matrix.

3.1. Secondary Control

The secondary control is realized by projecting a lower priority dynamic characteristic into the null space of the Jacobian. Previously, in refs. [8, 26, 27], a dynamic-level secondary task called Cartesian impedance control was realized in null space. A control law is devised for desired force and motion with a multi-priority impedance control in ref. [26]. In ref. [28], the dynamic coupling of macro and micro manipulator is investigated and it is deduced that higher frequency force or motion demands can be allocated to micro manipulator which improves the accuracy of the overall system. The algorithm proposed in this study is inspired by ref. [28] in terms of designing a virtual dynamic model (VDM) for the MMM to carry out secondary tasks. A decoupled control law is used for primary and secondary tasks by using the null-space projection of the Jacobian. The algorithm is designed to promote the distinct advantages of both manipulators. The VDM used for secondary tasks is used to regulate internal motions of manipulators, while the first task is carried out to track the desired end-effector trajectories. The VDM is presented in (18) by desired mass $\boldsymbol{M_d}$, damping $\boldsymbol{B_d}$, and stiffness $\boldsymbol{K_d}$ matrices.

$$\boldsymbol{M}_{\boldsymbol{d}}\ddot{\tilde{\boldsymbol{x}}} + \boldsymbol{B}_{\boldsymbol{d}}\dot{\tilde{\boldsymbol{x}}} + \boldsymbol{K}_{\boldsymbol{d}}\tilde{\boldsymbol{x}} = 0 \tag{18}$$

$$\tilde{\boldsymbol{x}} = \boldsymbol{x}_{\boldsymbol{Md}} - \boldsymbol{x}_{\boldsymbol{M}}, \dot{\tilde{\boldsymbol{x}}} = \dot{\boldsymbol{x}}_{\boldsymbol{Md}} - \dot{\boldsymbol{x}}_{\boldsymbol{M}}, \ddot{\tilde{\boldsymbol{x}}} = \ddot{\boldsymbol{x}}_{\boldsymbol{Md}} - \ddot{\boldsymbol{x}}_{\boldsymbol{M}} \tag{19}$$

where $\tilde{\boldsymbol{x}} \in \mathbb{R}^4$, $\dot{\tilde{\boldsymbol{x}}} \in \mathbb{R}^4$, and $\ddot{\tilde{\boldsymbol{x}}} \in \mathbb{R}^4$ error signal vectors are computed by subtracting the planar motions of the macro and micro manipulators, $\boldsymbol{x_M} \in \mathbb{R}^4$, $\dot{\boldsymbol{x}}_{\boldsymbol{M}} \in \mathbb{R}^4$, and $\ddot{\boldsymbol{x}}_{\boldsymbol{M}} \in \mathbb{R}^4$, from the desired planar motions, $\boldsymbol{x_{Md}} \in \mathbb{R}^4$, $\dot{\boldsymbol{x}}_{\boldsymbol{Md}} \in \mathbb{R}^4$, and $\ddot{\boldsymbol{x}}_{\boldsymbol{Md}} \in \mathbb{R}^4$.

A double mass-spring-damper model is used to describe the dynamic behavior of secondary task as shown in Fig. 2. The subscript 1 denotes the macro manipulator and the subscript 2 denotes the micro manipulator. The m_1 mass, k_1 spring constant, b_1 damping constant, and x_{M1} motion are used to represent the macro manipulator's VDM, while m_2 mass, k_2 spring constant, b_2 damping constant, and x_{M2} motion is used to represent the VDM of the micro manipulator. For each Cartesian axis (x- and y-axes in Fig. 1), a double mass-spring-damper model is used with the selected parameters

https://doi.org/10.1017/S0263574720000338 Published online by Cambridge University Press

that are discussed in the next section. With respect to these, VDM presented in Fig. 2 and its abovementioned parameters in (18) are calculated as follows:

$$\boldsymbol{M_d} = \begin{bmatrix} m_1 & 0 & 0 & 0 \\ 0 & m_1 & 0 & 0 \\ 0 & 0 & m_2 & 0 \\ 0 & 0 & 0 & m_2 \end{bmatrix}$$

$$\boldsymbol{K_d} = \begin{bmatrix} k_1 + k_2 & 0 & -k_2 & 0 \\ 0 & k_1 + k_2 & 0 & -k_2 \\ -k_2 & 0 & k_2 & 0 \\ 0 & -k_2 & 0 & k_2 \end{bmatrix} \tag{20}$$

$$\boldsymbol{B_d} = \begin{bmatrix} b_1 + b_2 & 0 & -b_2 & 0 \\ 0 & b_1 + b_2 & 0 & -b_2 \\ -b_2 & 0 & b_2 & 0 \\ 0 & -b_2 & 0 & b_2 \end{bmatrix}$$

Secondary joint acceleration demands are computed from VDM introduced in Eq. (18). First of all, (18) is reshaped as shown in Eq. (21).

$$\ddot{\boldsymbol{x}}_{\boldsymbol{M}} = \ddot{\boldsymbol{x}}_{\boldsymbol{Md}} + \boldsymbol{M_d^{-1}}[(\boldsymbol{B_d}\dot{\tilde{\boldsymbol{x}}} + \boldsymbol{K_d}\tilde{\boldsymbol{x}})] \tag{21}$$

An augmented Jacobian, $\boldsymbol{J_s} \in \mathbb{R}^{4x4}$, presented in Eq. (22) is formulated to relate the MMM's secondary joint space demands to VDM's task space motion which is the Cartesian motions of macro and micro manipulators.

First row in the matrix maps the *y*-axis demands of macro manipulator to the respective Cartesian space motion in *y*-axis. Second row in the matrix maps the *x*-axis demands of macro manipulator to the respective Cartesian space motion in *x*-axis. Third and fourth rows in the matrix map the active joint demands of micro manipulator to the respective Cartesian space motion in *y*- and *x*-axes, respectively.

$$\boldsymbol{J_s} = \begin{bmatrix} 0 & 1 & 0 & 0 \\ 1 & 0 & 0 & 0 \\ 0 & 0 & -\dfrac{l_3\sin(q_4+q_6)\sin(q_5)}{\sin(q_3+q_5-q_4-q_6)} & \dfrac{l_3\sin(q_3+q_5)\sin(q_6)}{\sin(q_3+q_5-q_4-q_6)} \\ 0 & 0 & \dfrac{l_4\cos(q_4+q_6)\sin(q_5)}{\sin(q_3+q_5-q_4-q_6)} & \dfrac{-l_4\cos(q_3+q_5)\sin(q_6)}{\sin(q_3+q_5-q_4-q_6)} \end{bmatrix} \tag{22}$$

Inverse kinematics is used to calculate the secondary joint acceleration demands, $\ddot{\boldsymbol{\theta}}$, by substituting (21) in (23) as shown in (24). Finally, the null-space vector is calculated by using null-space mapping in (25). With this simplified model in Eq. (18), the null-space vector, $\boldsymbol{\phi_N}$, to be used in (12) is found by computing secondary joint motion demands, $\ddot{\boldsymbol{\theta}}$.

$$\ddot{\boldsymbol{x}}_{\boldsymbol{M}} = \boldsymbol{J_s}\ddot{\boldsymbol{\theta}} + \dot{\boldsymbol{J}}_{\boldsymbol{s}}\dot{\boldsymbol{\theta}} \tag{23}$$

$$\ddot{\boldsymbol{\theta}} = \boldsymbol{J_s^{-1}}\{\ddot{\boldsymbol{x}}_{\boldsymbol{Md}} + \boldsymbol{M_d^{-1}}[(\boldsymbol{B_d}\dot{\tilde{\boldsymbol{x}}} + \boldsymbol{K_d}\tilde{\boldsymbol{x}})] - \dot{\boldsymbol{J}}_{\boldsymbol{s}}\dot{\boldsymbol{\theta}}\} \tag{24}$$

$$\boldsymbol{\phi_N} = (\boldsymbol{I} - \boldsymbol{J^+J})\ddot{\boldsymbol{\theta}} \tag{25}$$

In particular, secondary task demand, Eq. (24), represents a dynamic equation (VDM) expressed in terms of secondary task space variables projected to joint space by $\boldsymbol{J_s}$. By proper choice of the dynamic matrices $\boldsymbol{M_d}$, $\boldsymbol{B_d}$, and $\boldsymbol{K_d}$, it is possible to achieve the desired dynamic behaviors of macro and micro mechanisms without affecting the task-space dynamics and stability of the system. To achieve a stable system behavior in the null space of the system, the impedance-like controller's stability should be issued.

https://doi.org/10.1017/S0263574720000338 Published online by Cambridge University Press

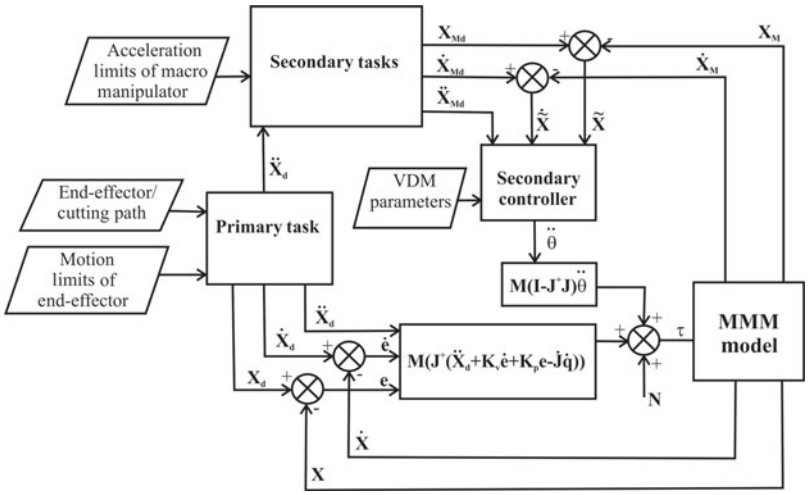

Fig. 3. The overall control scheme for the MMM.

The stability of the expression in Eq. (21) can be analyzed via the Lyapunov function $V = \frac{1}{2}\dot{\tilde{\boldsymbol{x}}}^{\boldsymbol{T}} \boldsymbol{M_d}\dot{\tilde{\boldsymbol{x}}} + \frac{1}{2}\tilde{\boldsymbol{x}}^{\boldsymbol{T}}\boldsymbol{K_d}\tilde{\boldsymbol{x}}$, where $\boldsymbol{M_d}$ and $\boldsymbol{K_d}$ are positive definite matrices. The derivative of Lyapunov function is obtained as $\dot{V} = -\dot{\tilde{\boldsymbol{x}}}^{\boldsymbol{T}}\boldsymbol{B_d}\dot{\tilde{\boldsymbol{x}}}$ from which it is concluded that the stability is preserved as $\boldsymbol{B_d}$ is positive definite. The defined virtual inertia $\boldsymbol{M_d}$, damping $\boldsymbol{B_d}$, and stiffness $\boldsymbol{K_d}$ determine the behavior of the robot when subjected to secondary control inputs.

The overall control scheme is illustrated in Fig. 3, where primary and secondary tasks and their information flow are distinctively shown. The primary task is created according to the trajectory generation of desired end-effector/cutting path and motion limits designated for the end-effector motion. The trajectory for the given path is planned by using the algorithm presented in ref. [21], which generates S-shaped velocity profiles to ensure finite jerk limits. The motion demands created from the primary task along with the position and velocity feedback of the end effector are used to generate error signals to be fed into the controller, which is explained in Eq. (12). The motion demand in the acceleration level is fed forward directly to the controller.

The secondary task block in Fig. 3 is used to distribute motion demands according to the acceleration and work space capabilities of the macro and micro manipulators. In this secondary task, the acceleration of the macro manipulator is constrained by complying with the work space limitation of the micro manipulator. The algorithm for such a distribution of motion demands is explained in detail in the next section.

A designed VDM, represented in Eq. (18), is used to formulate the secondary controller which is given in Eq. (23). The optimization of VDM parameters is described in the next section. The secondary controller's outputs, $\ddot{\boldsymbol{\theta}}$, are projected to null space, and $\boldsymbol{\phi_N}$ is issued as a controlled input to the actuators of the MMM model along with the other control inputs issued by the primary task's controller and the nonlinearity effects cancellation term $\boldsymbol{N}$.

Designing the system in this way allows adjusting the desired dynamic behaviors of MMM in a redundant configuration. The VDM parameters can be optimized depending on the acceleration and work space capabilities of the macro and micro manipulators. In this article, a case study is presented which optimizes these parameters for the MMM designed in ref. [21].

3.1.1. Secondary control tasks. The aforementioned secondary control tasks are achieved by designing the desired Cartesian space motions of macro and micro manipulators separately. For this application, the external forces acting on the secondary control is neglected in (21), because the algorithm is developed for a laser cutting machine in which the tool is never in physical interaction with its environment. Parameters of VDM ($\boldsymbol{M_d}$, $\boldsymbol{B_d}$, $\boldsymbol{K_d}$) should be optimized for the selected secondary tasks and the motion demands of this system $\ddot{\boldsymbol{x}}_{\boldsymbol{M1d}}, \ddot{\boldsymbol{x}}_{\boldsymbol{M2d}}$ should be accordingly set to achieve these secondary tasks. These tasks are selected as limiting the maximum acceleration of macro manipulator's axes and the work space for micro manipulator.

https://doi.org/10.1017/S0263574720000338 Published online by Cambridge University Press

Maximum acceleration limitation of the macro manipulator is achieved by saturating the desired end-effector acceleration demands to accomplish primary task. The primary task acceleration should be selected complying with the combined acceleration capabilities of the MMM. A saturation law is devised for the secondary task acceleration demands for the macro manipulator $\ddot{x}_{M1d}, \ddot{y}_{M1d}$ by saturating the motion demands for the end-effector's desired acceleration demands, $\ddot{\boldsymbol{x}}_{\boldsymbol{d}}$ along x- and y-axes. In (26) and (27), $\ddot{x}^{+}_{sat}$, $\ddot{y}^{+}_{sat}$ and $\ddot{x}^{-}_{sat}$ $\ddot{y}^{-}_{sat}$ are acceleration limits of macro mechanism which are set to accomplish +9.81 m/s^2 (+1 g) and -9.81 m/s^2 (-1 g) limitations, respectively.

$$\ddot{x}_{M1d} = \begin{cases} \ddot{x}^{+}_{sat}, & \ddot{x}_d \geq \ddot{x}^{+}_{sat} \\ \ddot{x}^{-}_{sat}, & \ddot{x}_d \leq \ddot{x}^{-}_{sat} \\ \ddot{x}_d, & else \end{cases}, \quad \ddot{y}_{M1d} = \begin{cases} \ddot{y}^{+}_{sat}, & \ddot{y}_d \geq \ddot{y}^{+}_{sat} \\ \ddot{y}^{-}_{sat}, & \ddot{y}_d \leq \ddot{y}^{-}_{sat} \\ \ddot{y}_d, & else \end{cases} \tag{26}$$

On the other hand, the micro manipulator's acceleration demands are generated to compensate for the difference between the primary task's assigned motion and the motion of macro manipulator. This is done by extracting the saturated macro manipulator demands from MMM's desired task trajectories in the Cartesian space.

$$\ddot{x}_{M2d} = \begin{cases} \ddot{x}_d - \ddot{x}^{+}_{sat}, & \ddot{x}_d \geq \ddot{x}^{+}_{sat} \\ \ddot{x}_d - \ddot{x}^{-}_{sat}, & \ddot{x}_d \leq \ddot{x}^{-}_{sat} \\ 0, & else \end{cases}, \quad \ddot{y}_{M2d} = \begin{cases} \ddot{x}_d - \ddot{y}^{+}_{sat}, & \ddot{x}_d \geq \ddot{y}^{+}_{sat} \\ \ddot{x}_d - \ddot{y}^{-}_{sat}, & \ddot{x}_d \leq \ddot{y}^{-}_{sat} \\ 0, & else \end{cases} \tag{27}$$

Hence, the secondary control task's acceleration demands, $\ddot{\boldsymbol{x}}_{\boldsymbol{Md}}$, are formed as shown in Eq. (28), which are the input signals of the secondary controller in Eq. (24). The velocity demands are calculated by integrating the acceleration demands for both manipulators, respectively.

$$\ddot{\boldsymbol{x}}_{\boldsymbol{Md}} = \begin{bmatrix} \ddot{x}_{M1d} \\ \ddot{y}_{M1d} \\ \ddot{x}_{M2d} \\ \ddot{y}_{M2d} \end{bmatrix} \tag{28}$$

Although a saturation on the acceleration level is implemented by using the above-mentioned methods, the algorithm still needs to guarantee that work space limitation of the five-bar planar micro manipulator is not violated. To ensure this, the VDM spring constants and springs' neutral position should be adjusted. For this study, to comply with the work space limitation of the micro manipulator, the neutral position of the spring in between the micro and macro manipulators is chosen at the middle position of the micro manipulator's work space by designing the position demand of the secondary control.

Designing the secondary task with VDM-based secondary control allows adjusting parameters to achieve both tasks at the same time. Also, by integrating a dynamic model, a continuous behavior of the secondary tasks is targeted in the presence of the discontinuity imposed by the saturation function.

3.1.2. Parameter optimization of secondary control objective. The VDM presented in Eq. (18) is designed to impose saturated accelerations and not to violate the work space of the micro manipulator. In this section, optimization of the VDM parameters is discussed. Parameters are optimized to meet the secondary control task explained in the previous section. To explain the optimization procedure, the VDM is analytically represented for only one Cartesian axis, which is, in the end, applied to both x- and y-axes.

Parameter optimization for the proposed model is realized by constructing a state-space representation of the VDM and running VDM parameter optimization with the selected performance index.

The VDM in state-space representation is given as follows:

$$\dot{\boldsymbol{z}} = \boldsymbol{A}\boldsymbol{z} + \boldsymbol{B}\boldsymbol{u} \tag{29}$$

https://doi.org/10.1017/S0263574720000338 Published online by Cambridge University Press

In Eqs. (30) and (31), state vector, z, and system matrix, $\boldsymbol{A}$, are defined as:

$$z = \begin{bmatrix} z_1 \\ z_2 \\ z_3 \\ z_4 \end{bmatrix} = \begin{bmatrix} x_{M1} \\ \dot{x}_{M1} \\ x_{M2} \\ \dot{x}_{M2} \end{bmatrix} \tag{30}$$

$$\boldsymbol{A} = \begin{bmatrix} 0 & 1 & 0 & 0 \\ -(k_1+k_2)/M_1 & -(b_1+b_2)/M_1 & k_2/M_1 & b_2/M_1 \\ 0 & 0 & 0 & 1 \\ k_2/M_2 & b_2/M_2 & -k_2/M_2 & -b_2/M_2 \end{bmatrix} \tag{31}$$

Optimization of VDM parameters consists of determining parameters k_1, k_2, b_1, and b_2 by minimizing the selected performance index, $\boldsymbol{W}$. For this problem, $\boldsymbol{W}$ penalizes state variables. In the conventional form, $\boldsymbol{W}$ would be formulated as follows:

$$\boldsymbol{W} = \int_0^\infty (z^T \boldsymbol{Q} z) dt \tag{32}$$

where $\boldsymbol{Q} \in \mathbb{R}^{4x4}$ is a positive definite weighting matrix. In conventional form, the $\boldsymbol{Q}$ matrix is given as:

$$z^T \boldsymbol{Q} z \triangleq -\frac{d}{dt} z^T \boldsymbol{R} z \tag{33}$$

$$-\boldsymbol{Q} = \boldsymbol{A}^T \boldsymbol{R} + \boldsymbol{R}\boldsymbol{A} \tag{34}$$

where $\boldsymbol{R} \in \mathbb{R}^{4x4}$ is a symmetric matrix. In this work, $\boldsymbol{W}$ is modified, so that accelerations of masses are included with term, $\ddot{\tilde{z}}$.

$$\boldsymbol{W} = \int_0^\infty (z^T \boldsymbol{Q} z + \ddot{\tilde{z}}^T \boldsymbol{S} \ddot{\tilde{z}}) dt \tag{35}$$

Based on the VDM, accelerations are calculated by $\begin{bmatrix} \ddot{x}_{M1} \\ \ddot{x}_{M2} \end{bmatrix} = \boldsymbol{V} z$, where the matrix $\boldsymbol{V}$ is defined as follows:

$$\boldsymbol{V} = \begin{bmatrix} -(k_1+k_2)/M_1 & -(b_1+b_2)/M_1 & k_2/M_1 & b_2/M_1 \\ k_2/M_2 & b_2/M_2 & -k_2/M_2 & -b_2/M_2 \end{bmatrix} \tag{36}$$

Making use of the abovementioned relation, $\boldsymbol{W}$ is rewritten as follows:

$$\boldsymbol{W} = \int_0^\infty z^T \left(\boldsymbol{Q} + \boldsymbol{V}^T \boldsymbol{S} \boldsymbol{V}\right) z \, dt \tag{37}$$

At this moment, we can define a new weighting matrix $\boldsymbol{Q}_s$ in Eq. (38).

$$\boldsymbol{Q}_s = \boldsymbol{Q} + \boldsymbol{V}^T \boldsymbol{S} \boldsymbol{V} \tag{38}$$

where $\boldsymbol{S}$ is a weighting matrix which is chosen to impose minimization for only macro manipulator's acceleration.

$$-\boldsymbol{Q}_s = \boldsymbol{A}^T \boldsymbol{R} + \boldsymbol{R}\boldsymbol{A} \tag{39}$$

The $\boldsymbol{R}$ matrix is a function of VDM parameters. Finally, the optimal solution is found by the minimization of $\boldsymbol{W}$.

$$\boldsymbol{W} = z^T \boldsymbol{R} z \tag{40}$$

https://doi.org/10.1017/S0263574720000338 Published online by Cambridge University Press

Table II. Parameters of VDM.

	Initial values of parameters	**Optimized values of parameters**
k_1	0	1.61
k_2	12	10.28
b_1	35	58.07
b_2	1	4.46

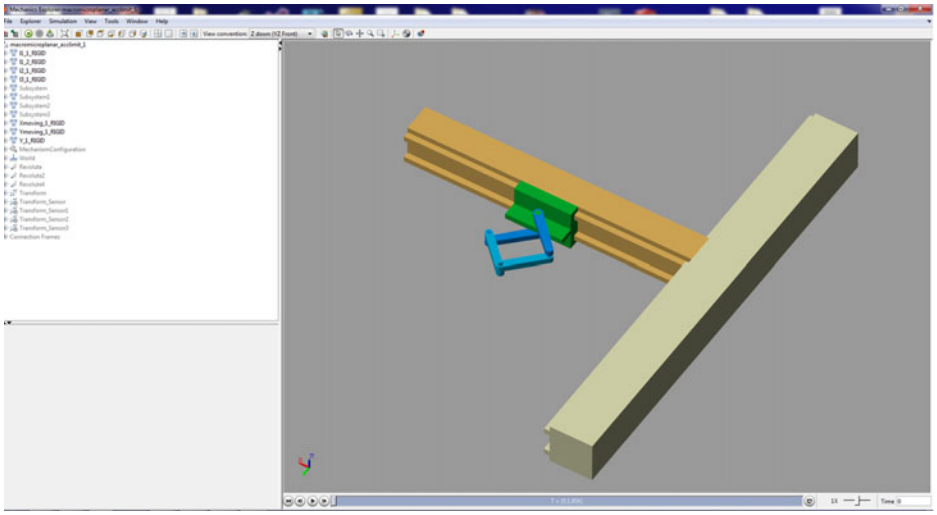

Fig. 4. Visualization of simulations done with Matlab™ Simscape™ Multibody™ model.

$\boldsymbol{W}$ is subjected to the Nelder–Mead optimization method using Matlab functions to find minimum of the constrained nonlinear multivariable function. A local minimum is found for parameters given in Table II with initial conditions and constraints with upper and lower bounds of parameters as $0 < k_1 < 10$, $0 < k_2 < 100$, $0 < b_1 < 100$, $0 < b_2 < 100$. It is known that with different initial parameters, the parameters for resultant minima changes, because of this the initial values are set manually by trial and error by making use of simulation test results to accomplish secondary tasks with more precision.

As a result, the system matrix $\boldsymbol{A}$ with optimized parameters (Table II) has eigenvalues of $-2.2567 + 2.2984i$, -2.2567, -2.2984, -0.0291, *and* -0.5460. It should be noticed that the real part of eigenvalues of the system matrix $\boldsymbol{A}$ used in the simulations are all negative, which shows that the system satisfies the condition of stability. The parameters obtained with this optimization are used in the controller and tested in simulations, which are presented in the next section.

4. Simulation and Results

A case study is presented to show the performance and viability of the proposed method. Simulation model is constructed by using Matlab ™ Simscape™ Multibody™ blocks. A simplified model of the MMM presented in ref. [22] with the physical parameters presented in Table I is built in this simulation environment and its visual representation is presented in Fig. 4. Initially, a dynamic analysis of the MMM is carried out and validated with the results of the model constructed with Matlab™ Simscape™ Multibody™ blocks. This validated model is used in computing the respective matrices (e.g., generalized inertia matrix) in the computed torque method which is implemented as the control law for the primary task. Simulations are run with 2 kHz sampling rate and with ODE4 (Runge–Kutta) solver.

The contour that was studied previously in ref. [22], shown in Fig. 5, for the end-effector's trajectory is used for the planar laser cutting process as the benchmark test of the proposed controller. For this contour, the trajectory is generated with 40 m/min velocity, 4150 m/s^3 jerk, and 43.13m/s^2 acceleration limits. These values are assigned with respect to the aimed capabilities of

https://doi.org/10.1017/S0263574720000338 Published online by Cambridge University Press

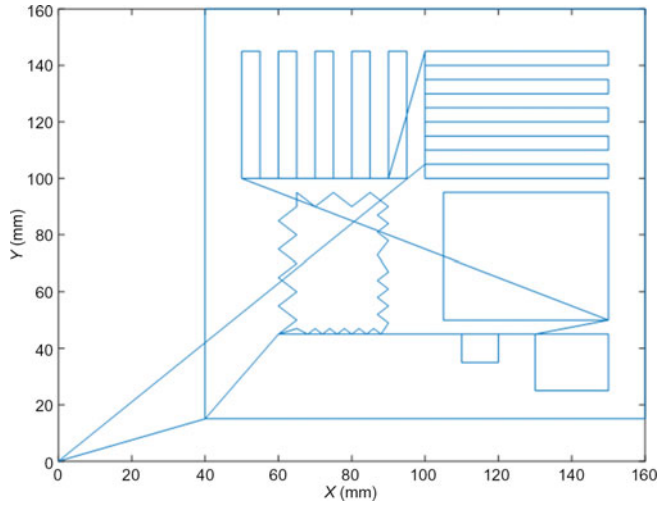

Fig. 5. End-effector path used in simulations.

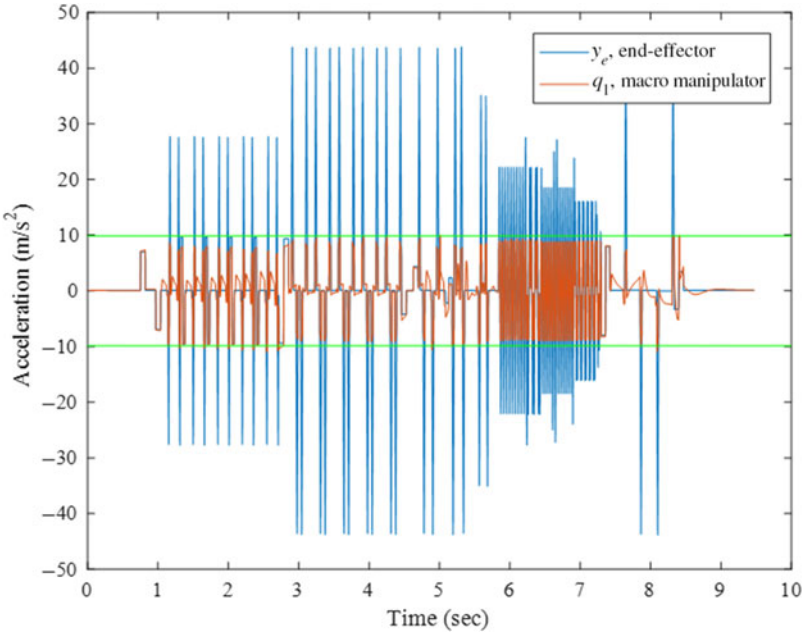

Fig. 6. Macro mechanism's q_1 joint accelerations and end-effector's accelerations along y-axis.

the MMM in refs. [21, 22]. The trajectory for the primary task is planned to have S-shaped velocity profiles as explained in ref. [21] for finite jerk limits.

With the abovementioned limitations of the MMM, the task completion duration is calculated to be 7.22 s. The same trajectory with the conventional machine (only the macro manipulator) with 1 g acceleration limitation is calculated to be completed in 11.27 s. This result indicates that there is a 35.93% drop in the total task completion duration if the acceleration levels are increased for this case study. Obviously, as the cutting path would have more small contours, the task completion duration decreases relative to the conventional machine's completion duration as reported in refs. [21, 22].

The controller is tested with the integrated secondary controller to investigate the impact of the proposed algorithm. Figs. 6 and 7 show the accelerations realized along the global y- and x-axes, respectively, which are drawn for the macro manipulator's axes (q_1 and q_2) and end-effector's axes (x_e and y_e). It is observed from Figs. 6 and 7 that the macro manipulator actuators' accelerations are kept within 1 g limitation (highlighted in figures with the green lines) along both axes. This result indicates that the first task of the secondary controller has been accomplished for limiting the acceleration of the macro manipulator.

https://doi.org/10.1017/S0263574720000338 Published online by Cambridge University Press

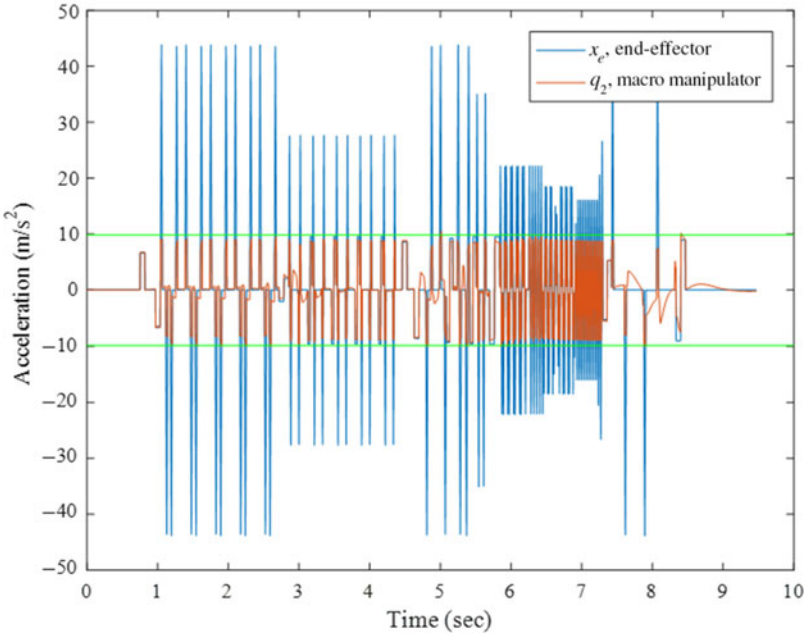

Fig. 7. Macro mechanism q_2 joint accelerations and end-effector's accelerations along x-axis.

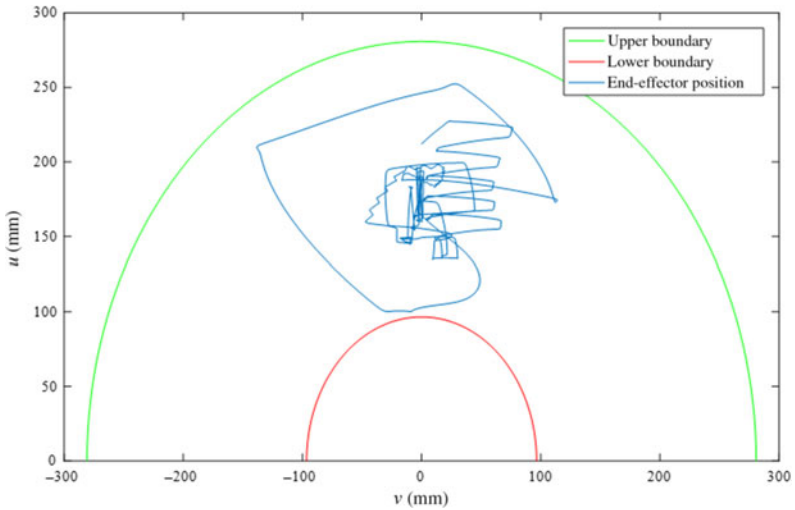

Fig. 8. End-effector position with respect to micro manipulator's fixed axes.

The second task of the secondary controller is used to keep the motion of the micro manipulator within its work space boundaries. The result of the micro manipulator motion in terms of u-v coordinates of the end effector with respect to the frame that is fixed to the micro manipulator is presented in Fig. 8. This figure indicates that the work space boundaries are not violated during the operation and the second task of the secondary controller is also accomplished.

The same trajectory is run for the conventional case (while only macro manipulator's joints are activated) where the motion limits in terms of acceleration and jerk are kept the same. In reality, the trajectory generated for the combined motion capability of MMM is not feasible for the conventional machine since it would call for much larger actuation capacity to move large amount of moving mass at the selected motion limits. However, in order to compare the effectiveness of the MMM with the proposed algorithm with a conventional machine, the simulation tests are repeated with the conventional machine by using the same motion limits. As a result, the total actuator effort calculated as drawn power by the total system with the MMM and conventional machine are shown in Fig. 9. It should be noted that the friction models are not included in the simulation model of both machines. It is clear that the effort is considerably lower when the MMM is used for the same task instead of

https://doi.org/10.1017/S0263574720000338 Published online by Cambridge University Press

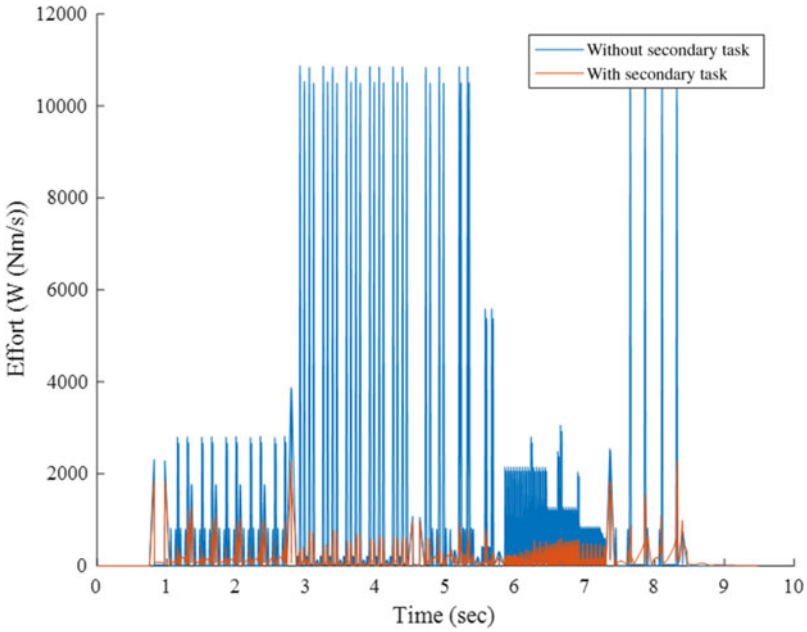

Fig. 9. Total actuator efforts for two simulation cases.

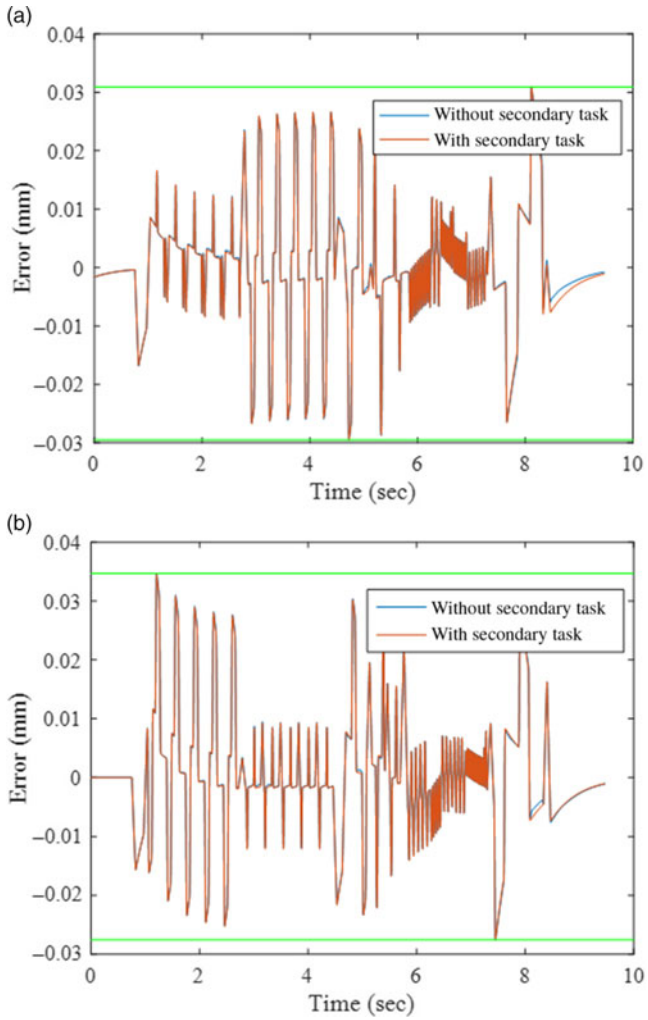

Fig. 10. End-effector position error (a) in *y*-direction (b) in *x*-direction.

https://doi.org/10.1017/S0263574720000338 Published online by Cambridge University Press

the conventional machine. The total energy consumed when the MMM is used is 2397.82 J, while it is 8118.56 J for the conventional machine for this specific task.

The end-effector positioning errors calculated for both the MMM and the conventional machine simulation tests are shown in Fig. 10. The positioning errors are bounded for both cases within 0.035 mm throughout the motion. The maximum positioning error is found to be 0.0347 mm. Positioning errors for both machines are found to be similar, hence it can be deduced that secondary control does not affect the primary task, which is tracking the end-effector's assigned trajectory.

5. Conclusions

For a laser cutting process, the laser head/end-effector velocity limitations are determined with the laser power and workpiece specifications (material and thickness). Increasing the acceleration of the end-effector's motion is one way to reduce the task completion duration. In the previous studies, the MMM concept was used to increase the acceleration capability of the laser cutting process in order to shorten the task completion duration. In this concept, a relatively lightweight and more agile micro manipulator attached to the conventional macro manipulator is utilized to increase the acceleration capability with combined motions of MMM. In this study, the macro manipulator is set as a conventional *x*-*y* table and the micro manipulator is designed as a five-bar parallel planar mechanism based on the industrial machine presented in ref. [21].

The major contribution of this article is the implementation of a control algorithm utilizing redundancy resolution for the MMM. A multi-priority controller making use of virtual dynamics, which is a double mass-spring-damper system, is introduced in null-space projection to achieve two desired secondary tasks. The primary task is set as end-effector trajectory tracking which is realized with computed torque control. Moreover, a secondary task is designed to distribute the acceleration demands of the end effector to macro and micro manipulators, complying with their acceleration and work space capabilities.

The algorithm is tested in simulations using a model based on the industrial setup presented in ref. [21]. A trajectory is designed according to the selected motion limitations of the MMM, so that the task completion duration is reduced by 35.93% with respect to the conventional machine operation. The test results indicate that the secondary tasks for keeping the macro manipulator's acceleration below 1 g and not violating the micro manipulator's work space are accomplished. These results prove that the design algorithm can be used in MMM systems in which the acceleration and work space limits are to be regulated.

When compared to the previously devised algorithm in ref. [21] which is tested on an industrial setup, the proposed algorithm is not task-specific. The virtual dynamics (double mass-spring-damper) utilized in the secondary controller makes the control of MMM versatile since the parameters and even the VDM can be adjusted to obtain the desired internal behavior of a redundant robot in MMM configuration. The control strategy along with the MMM concept introduced here can be utilized for various sub-task strategies in MMMs. The results achieved in this paper can be extended to the generation of anthropomorphic motions for MMMs that imitate human arm–wrist motions.

Another difference of this new algorithm is that it enables online control without the need to process desired end-effector trajectory, which overcomes many problems in the previous study. Specifically, if a trajectory is paused during an operation, the trajectory must be re-calculated with the previously studied preprocessing algorithms. However, with the algorithm proposed in this article, the trajectory tracking can be reinitiated at any moment.

Finally, if the same trajectory is cut with only the macro mechanism, with the same end-effector motion constraints, it is seen that actuator effort is increased relative to the results obtained with the MMM that uses the proposed algorithm. The effectiveness of the proposed method in terms of actuator effort is maximized when contours of the cutting path are relatively small and complex. The actuator effort is mainly reduced as a result of saturating macro manipulator's accelerations by using the secondary controller. The main reason to focus on the macro manipulator's acceleration is that the macro manipulator has relatively larger inertia and mass and, therefore, higher influence relative to the micro manipulator in terms of energy consumption.

Acknowledgments

This work is supported by The Scientific and Technological Research Council of Turkey via grant number 116M272.

References

1. Y. Nakamura, H. Hanafusa and T. Yoshikawa, "Task-priority based redundancy control of robot manipulators," *Int. J. Robot. Res.* **6**(2), 3–15 (1987).
2. G. F. Liu, Y. L. Wu, X. Z. Wu, Y. Y. Kuen and Z. X. Li, "Analysis and control of redundant parallel manipulators," *Proceedings of IEEE International Conference on Robotics and Automation*, Seoul, South Korea (May 2001) pp. 3734–3741.
3. H. Seraji, "Task options for redundancy resolution using configuration control," *Proceedings of 30th IEEE Conference on Decision and Control*, Brighton, UK (December 1991) pp. 2793–2798.
4. T. Petriè and L. Žlajpah. "Smooth continuous transition between tasks on a kinematic control level: Obstacle avoidance as a control problem," *Robot. Auton. Syst.* **61**(9), 948–959 (2013).
5. E. Tatlıcıoğlu, D. Braganza, T. C. Burg and D. M. Dawson, "Adaptive control of redundant robot manipulators with subtask objectives," *Robotica* **27**(6), 873–881 (2009).
6. O. Maaroof, E. Gezgin and M. İ. C. Dede, "General Subtask Controller for Redundant Robot Manipulators," *IEEE Proceeding of the 12th International Conference on Control, Automation and Systems, (ICCAS)*, JeJu Island, South Korea (October 2012) pp. 1352–1357.
7. L. Sentis and O. Khatib, "Prioritized multi-objective dynamic controller for robots in human," *Proceedings of the IEEE/RAS International Conference on Humanoid Robots*, Santa Monica, CA, USA (2004) pp. 764–780.
8. H. Sadeghian, L. Villani, M. Keshmiri and B. Siciliano, "Dynamic multi-priority control in redundant robotic systems," *Robotica* **31**(7), 1155–1167 (2013).
9. A. Dietrich, C. Ott and A. Albu-Schäffer, "An overview of null space projections for redundant, torque-controlled robots," *Int. J. Robot. Res.* **34**(11), 1385–1400 (2015).
10. J. Huang, B. T. Quan, M. Harada and T. Yabuta, "Emulating the Motion of a Human Upper Limb: Controlling a Finger-Arm Robot by Using the Manipulability of Its Finger," *Proceeding of IEEE International Conference on Robotics and Biomimetics*, Kunming, China (December 2006) pp. 607–612.
11. A. Sharon and D. Hardt, "Enhancement of Robot Accuracy Using Endpoint Feedback and a Macro-Micro Manipulator System," *Proceedings of 1984 American Control Conference*, CA, USA (June 1984) pp. 1836–1842.
12. O. Khatib, "Reduced Effective Inertia in Macro-/Mini-Manipulator Systems," **In:** *Robotics Research 5* (H. Miura and S. Arimoto, eds.) (MIT Press, Cambridge, 1990) pp. 279–284.
13. S. Arifin, M. H. Ang, C. Y. Lai and C. W. Lim, "General Framework of the Force and Compliant Motion Control for Macro Mini Manipulator," *Proceedings of 2013 IEEE/ASME International Conference on Advanced Intelligent Mechatronics*, Wollongong, NSW, Australia (July 2013) pp. 949–954.
14. T. Yoshikawa, T. Harada and A. Matsumoto, "Hybrid position/force control of flexible-macro/rigid-micro manipulator systems," *IEEE Trans. Robot. Aut*. **12**(4), 633–640 (1996).
15. H. Chen, J. Li, G. Xing, J. Xing and H. Sun, "Trajectory Tracking Control of a Macro-Micro Welding Robot Based on the Vision Navigation," *IEEE International Conference on Robotics and Biomimetics*, Tianjin, China (December 2010) pp. 667–672.
16. S. Arifin, M. H. Ang, C. Y. Lai and C. W. Lim, "General Framework of the Force and Compliant Motion Control for Macro Mini Manipulator," *Proceedings of 2013 IEEE/ASME International Conference on Advanced Intelligent Mechatronics*, Wollongong, NSW, Australia (July 2013) pp. 949–954.
17. Z. Ma, G. S. Hong, M. H. Ang and A. N. Poo, "Design and Control of An End-Effector Module for Industrial Finishing Applications," *2016 IEEE International Conference on Advanced Intelligent Mechatronics (AIM)*, Banff, AB, Canada (July 2016) pp. 339–344.
18. P. Leibinger, T. Rauser and L. Zeygerman, "Laser Cutting Machine with Multiple Drives," Patent No: US20040178181 (2004).
19. Sartorio, F., "Machine Tool and Manipulator Devise Adapted to be Mounted on Such Machine," Patent No: US20040025761 (2004).
20. M. Gattiglio, F. Sartorio and M. Chirico, "Laser Machine Tool," Patent No: US20080197118 (2008).
21. E. Uzunoğlu, M. İ. C. Dede and G. Kiper, "Trajectory planning for a planar macro-micro manipulator of a laser-cutting machine," *Ind. Robot* **43**(5), 513–523 (2016).
22. M. İ. C. Dede, G. Kiper and E. Uzunoğlu, "A Macro-Micro Mechanism Design for Laser Cutting Process," *17th International Conference on Machine Design and Production*, Bursa, Turkey (July 2016) pp. 71–85.
23. F. Ghorbel, O. ChBtelat and R. Longchamp, "A Reduced Model for Constrained Rigid Bodies with Application to Parallel Robots," *Proceedings of 4th IFAC Symposium on Robot Control*, Capri, Italy (September 1994) pp. 57–62.
24. F. Ghorbel, "Modeling and PD Control of a Closed-Chain Mechanical System," *Proceedings of 1995 34th IEEE Conference on Decision and Control*, New Orleans, LA, USA (December 1995) pp. 540–542.
25. P. Hsu, J. Hauser and S. Sastry, "Dynamic Control of Redundant Manipulators," *J. Robot. Syst.* **6**(2), 133–148 (1989).
26. R. Platt Jr., M. Abdallah and C. Wampler, "Multiple Priority Cartesian Impedance Control," *Proceedings of IEEE International Conference on Robotics and Automation*, Shanghai, China (May 2011) pp. 6033–6038.
27. F. Vigoriti, F. Ruggiero, V. Lippiello and L. Villani, "Control of redundant robot arms with null-space compliance and singularity-free orientation representation," *Robot. Auton. Syst.* **100**, 186–193 (2013).
28. A. Sharon, N. Hogan and D. E. Hardt, "The macro-micro manipulator an improved architecture for robot control," *Robot. Comput. Integr. Manuf.* **10**(3), 209–222 (1993).